Modeling of soil water retention based on 3D micro-tomographic image analysis

JAT de Oliveira*, L F Pires, FAM Cássaro, A M Brinatti & S C Saab

Laboratory of Soil Physics and Environmental Sciences, Department of Physics, State University of Ponta Grossa (UEPG),
Av. Carlos Cavalcanti, 4748, CEP 84.030-900, Ponta Grossa, PR, Brazil

This paper proposes the use of an algorithm based on the mercury intrusion porosimetry (MIP) method to obtain the water retention characteristic curve (pF curve) of a soil under different treatments. 3D X-ray micro-tomographic images were used to quantify pore size distribution, which was employed for the evaluation of the water retention in different matric potentials. The results showed very good agreement between the traditional method (obtained by suction tables) and that one based on the MIP algorithm. It means that the use of simulation procedures can be an interesting alternative for the measurement of soil water retention properties.

1 Introduction

Porous systems such as rocks and soils tend to present great complexity when analyzed in micrometric and nanometric scales[1]. Soils are generally characterized by complex pore arrangements, mainly in their top-layers, where the flora and the fauna have a more direct action[2].When submitted to contrasting management systems, soil structural properties can present important changes due to the action of soil preparation[3,4]. The conventional management system, one of the soil preparation techniques employed in Brazil, can greatly affect the soil pore system due to harrowing and plowing operations carried out on its surface layers[5-7].

Conventional managements modify the soil structure by employing operations for removing plant residues from the previous crops[7]. Soil porosity, bulk density, water retention, and aggregate stability are some of the properties largely influenced by conventional management systems, mainly on its surface layer[8,9]. At the micrometric scale, pore space geometry is also significantly affected by management systems[10,11].

The complexity of the soil porous system across different scales, and especially at the micrometer level, has important consequences for the environment, since it can contribute to carbon and other greenhouse gas sequestration[12]. Water retention, storage, and movement are largely affected by the architecture of the porous system of the soil. It also plays an important role in water infiltration, preventing damages to the soil structure due to, for example, erosion processes[7].

One important property that is directly influenced by changes in the soil structure is the water retention curve (pF curve). The pF curve, that relates the matric potential and the soil water content in the soil, is used to assess the soil physical quality and also employed as an indicator for improving soil management procedures[13]. Usually, regression models utilized for fitting the pF curve also permitan indirect estimation of the pore size distribution curve (PSD). It is accomplished by analyzing the first derivative of the fitted pF curve[14-16].

The experimental procedures to obtain a complete pF curve are generally time-consuming (months), laborious, and subject to several types of problems and experimental limitations. Therefore, it is desirable to find alternatives for its evaluation[17]. In the last decades, techniques based on image analysis have appeared as important tools to characterize complex systems mainly due to the use of more powerful computers and software of analysis dedicated to the investigation of porous systems[2,18-20].

Nowadays, methods based on three-dimensional (3D) image analysis have enabled the study of the architecture of the soil pores across different scales[21]. Researchers worldwide have worked on computer simulations based on micro-tomographic (μCT) images aiming at quantifying the physical properties

---

*Corresponding author: (E-mail: jossajato@gmail.com)

of different porous media[2,18,22]. The µCT data can be used to determine soil hydraulic properties like the pF curve, which is an important parameter to infer the quality of the soil. Algorithms based on experimental techniques such as mercury intrusion porosimetry (MIP) can be utilized to simulate water retention properties[23]. One of the advantages is related to these simulations being carried out in the preserved porous space of the samples under evaluation[22].

Thus, the objective of this work was to examine the ability of an algorithm based on MIP to determine partial pF curves. Samples of soil under native forest and submitted to a conventional tillage procedure were analyzed and compared. Three-dimensional (3D) microtomographic images were used together with the computer method developed by Yang *et al.*[23] to obtain PSDs and, subsequently, pF curves.

2 Experimental Details

The experimental plot where the samples were collected is located at the Agronomic Institute of Parana (25° 09' S, 50° 09' W, 875 m a.s.l). The samples were collected in adjacent areas under conventional tillage (CT) and secondary forest (Ft)(the latter issued as a reference). The soil is classified as a Rhodic Hapludox according to the Soil Survey Staff[24,25].

Seven samples (n=7) were collected at the top-layer (0-0.10 m) for each treatment (Ft and CT). For CT, soil samples were collected six months after plowing-harrowing operations and corn harvesting. The Rhodic Hapludoxin this study presented contents of clay, silt, and sand as follows: 578 g kg^{-1}, 280 g kg^{-1}, and 142 g kg^{-1} (Ft) and 610 g kg^{-1}, 220 g kg^{-1}, and 170 g kg^{-1} (CT), which indicates only marginal differences in their textures.

An X-ray microtomographic system model v|tomex|m (GE) from the Hounsfield Facility (The University of Nottingham), operating at 180 kV and 160 µA, was employed to scan the samples. The 3D soil pore system reconstruction was created by stacking 860 2D images (35µm of pixel size). This generated a volume of interest of about 30×30×30 mm[3]. The Otsu non-parameterized method (*ImageJ* 1.42) was used to obtain image threshold and segmentation according to the procedures adopted by Pires *et al.*[2].

The pore size distribution (PSD) was obtained through the method presented by Yang *et al.*[23]. The PSD is represented by the frequency of pores of any characteristic diameter "D" that was detected in the Yang procedure:

$$PSD = \frac{V_{diameters}}{V_{overall}} \equiv f(D) \qquad \dots (1)$$

where $V_{overall}$ represents the volume of the reconstructed sample.

The pF curve was obtained based on the PSDs (pFcurve$_{PSD}$) using Equation 2 that represents the cumulative sum of pore frequencies of some characteristic diameters:

$$pFcurve_{PSD} = \sum_{D_i}^{D_j} f(D) \qquad \dots (2)$$

where D_i and D_j ($D_i > D_j$) are two characteristic diameters of interest.

The experimental pF curves (pFcurve$_{Exp}$) were obtained using a tension table EijKelkamp®, model 08.01 SandBox. After being saturated using the capillary rise method, the samples were submitted to matric potentials that varied from 1 to 10 kPa (considering the modulus of Ψ), in step intervals of 1 kPa. The matric potential of 10 kPa allowed to access pores with approximately 30 µm of equivalent cylindrical diameter. Regarding pFcurve$_{PSD}$, due to the spatial resolution of the images, the analysis was restricted to approximately 70 µm (≈4.3 kPa).

The porosity(ϕ)was calculated by the area below the PSD curve considering the largest (D_{max}) and the smallest (D_{min}) ($D_{max}>D_{min}$) pores within $V_{overall}$:

$$\phi = \left(\sum_{D_{min}}^{D_{max}} \frac{V_{diameters}}{V_{overall}} \right) 100 \qquad \dots (3)$$

The matric potential was obtained through the Yang-Laplace equation:

$$|\Psi| = \frac{298}{D} \qquad \dots (4)$$

The pFcurve$_{PSD}$ and pFcurve$_{Exp}$ curve data were interpolated using the van Genuchten (VG) equation with the Mualem restriction $\left(m = 1 - \frac{1}{n} \right)$[15]:

$$\theta = \theta_r + \frac{(\theta_s - \theta_r)}{[1 + (\alpha h)^n]^m} \qquad \dots (5)$$

where θ_s and θ_r represent the saturated and residual volumetric water contents, α, n and m are adjustment parameters of the VG equation .The coefficient of correlation (R^2) was utilized to verify the pF curve data interpolation quality.

3 Results and Discussion

The three-dimensional images show that the structure of the soil under CT exhibited more

diversified groups of pores as compared to Ft, which is probably associated with the soil disturbance under this management system[4] (Fig. 1).After the aggregates breakdown (produced in the harrowing and plowing operations), the soil under CT usually has its porosity increased, which tends to favor an increment in the number of rounded shapedpores[26,27]. In Ft, the presence of connected and longer pores is probably a consequence of the biological activity in the soil surface layers as shown in the tomographic images. The existence of large rounded shaped pores is associated with the action of the root development and the fauna activity of the porous system under Ft (biopores)[12].

However, the connectivity (data not shown) was higher in the CT due to the breakdown of the aggregate structure in the harrowing and plowing operations and further reconsolidation of the soil surface[2]. Recently, Borges et al.[11] working at the same experimental field also found higher values of connectivity for CT in relation to Ft for the sub-surface layer. Despite the aggregate breakdown induced in CT, the reconsolidation of soil surface layers due to the action of wetting and drying cycles in the experimental area studied favoured the connection of the pores throughout time. Nonetheless, both treatments were characterized by well-connected pore systems (Fig. 1).

According to what was previously discussed, soils under both treatments are not compacted. Usually, areas under CT might suffer compaction associated with the mechanical harvesting and other operations due to the traffic of agricultural machinery. Bulk densities found for Ft and CT were 0.90g cm^{-3} and

0.99 g cm^{-3}, respectively. Reichert et al.[28]pointed out that compacted soils, for different soil preparation and clay textures in Brazil, present bulk density values around 1.21 g cm^{-3}. Therefore, the values presented here clearly show that CT soils are not compacted, helping to explain the highest accessed porosity by the image obtained. Values close to those determined here, for a Rhodic Hapludox under Ft and CT, were also reported by da Costa et al.[29].

PSDs obtained via the methodology based on MIP for the samples submitted to Ft and CT are shown in Fig. 2. It is noticeable that the curves are dissimilar in

Fig. 2 — (a) Pore size distribution obtained via 3D image analysis, (b,c) Partial soil water retention curves determined by the traditional method (Exp) and based on 3D image analysis (PSD). Ft: Forest; CT: Conventional Tillage; F(%): Frequency of pores; D: Diameter of the pores; θ: Soil water content; $|\Psi|$: Matric Potential.
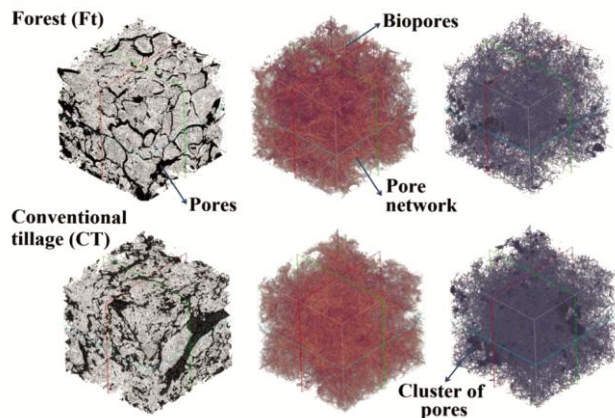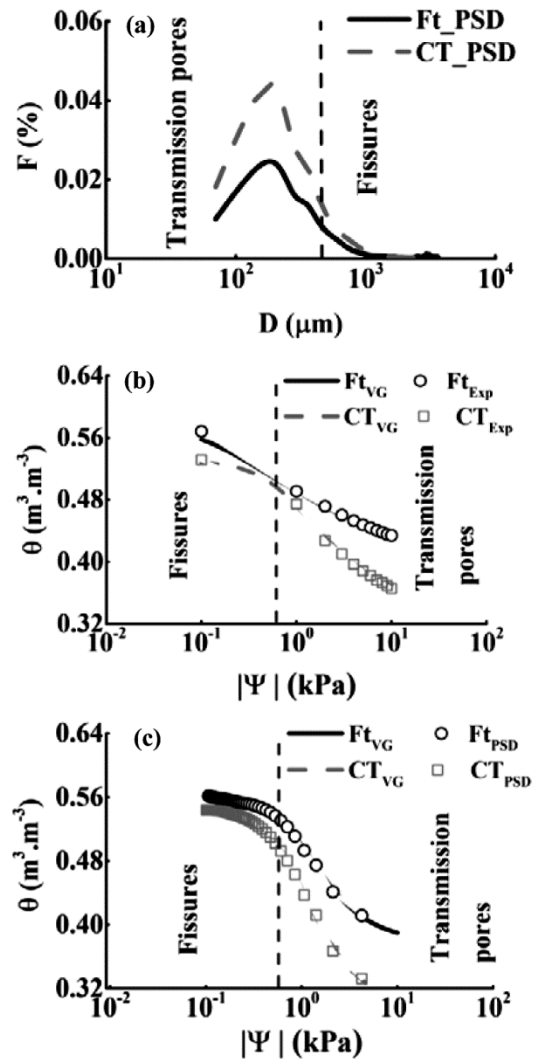

Fig. 1 — X-ray microtomographic images of soil cores. The images in yellow show the pore network and the images in green exhibit the skeleton of the porous system.

their amplitudes, and CT is the highest one (Fig. 2a). The porosities, given by the areas below the PSD curves, were significantly different(Student's t-test, p<0.05) between treatments (Ft: 14% and CT: 23%).It seems relevant to highlight that the previous porosities are the porosities accessed by the analysis of micro-tomographic images, and, due to the resolution of the images, only macropores were detected and quantified. Therefore, the porosity accessed by image, in this case, was limited to only 40% of the total porosity observed in the pFcurve$_{Exp}$ (Figs. 2(a-b)). The total porosity, which sometimes can be assessed by θ_r, for both treatments, mainly by the traditional method, includes a portion of micropores (pore diameters <50 μm), influencing water retention and total porosity values. In this study, even being restricted to macropores, the analysis showed that the number of pores with characteristic sizes between 70 (≈4.3kPa) and 1000 (≈0.3 kPa) μm was significantly greater for CT as compared to Ft (Fig. 2a)[6,10,16,29-30].

The porous system is also primarily composed of transmission pores (D < 500 μm) (Ft: 72% and CT: 79%), which are structural pores responsible for air movement and water drainage in the soil matrix[16]. The appearance of more transmission pores in CT as compared to Ft certainly contributed favorably to the higher value of the total porosity accessed by image analysis (Fig. 1). A small proportion of the accessed porosity was related to fissures (D > 500 μm) (Ft: 28% and CT: 21%). In the water movement process, fissures are essentially related to water infiltration at high velocities[31]. The largest proportion of fissures for CT can be explained by the presence of the pore cluster as observed in the 3D images (Fig. 1).

The pF curves derived from the simulated PSD and the traditional method showed reasonable agreement, mainly in the lower matric potential range, as shown in Figs. 2(b), (c)[23]. The pF curve for the treatments (Ft and CT) had slight differences in the region of larger pores (fissures), which is probably related to the presence of connected macropores in the soil porous system[2,10]. The soil revolving procedure affected mainly the pores of intermediate sizes (transmission pores, D<500 μm). This means that the soil structure changes induced by CT mainly influenced the pores linked to water redistribution, conduction, and storage[32]. However, it is important to mention that, regardless of the treatment, Yang´s approach was efficient in modeling the water retention curve. The close relation between the pF curves (obtained by the traditional and the simulated methods) corroborates it (Table 1).

The agreement between the two methods is mainly verified by the proximity of the values of saturation and residual soil water contents shown in Table 1, and also, by the quality of the mathematical model adjustment considering the high values of the correlation coefficients (R^2). The largest difference between F curves was around 15% and occurred from potentials ranging from 6 to 10 kPa. The CT results showed that the approach resulted in differences of about 17%, also for smaller pores, related to potentials ranging from 7 to 10 kPa. For larger pores these differences dropped to something around 0%. The measurement of pore volume inside the soil samples resulted in feasible results of water distribution in 3D based on image analysis[20]. The low agreement between the curves pF for high matric potentials is justified by the limited resolution capacity of the microtomographic images of the samples used in the Yang's procedure, and subsequently in the pFcurve$_{PSD}$ determinations.

Graphics of the amount of water retained by the soil for the different treatments, evaluated by the traditional and the Yang´s method are presented in Figs. 3(a-b). It seems relevant to mention that for both Ft and CT, the Yang approach underestimated the amount of water retained in the porous media investigated, especially for the regions of lower

Table 1 — Parameters of the van Genuchten model for the mathematical adjustment of the water retention curves (Exp: Experimental and PSD: Yang´s model).

Treatment	θ_s	θ_r	α	n	m	θ_s-θ_r	R^2
	(m^3 m^{-3})	(m^3 m^{-3})	(kPa^{-1})			(m^3 m^{-3})	
Ft$_{Exp}$	0.58	0.36	6.91	1.26	0.2	0.14	0.99
Ft$_{PSD}$	0.56	0.38	1.06	2.12	0.53	0.18	0.99
CT$_{Exp}$	0.53	0.34	1.18	1.74	0.43	0.16	0.99
CT$_{PSD}$	0.55	0.29	1.23	2.15	0.53	0.21	0.99

Ft: Forest; CT: Conventional Tillage; θ_s: Saturated volumetric water content; θ_r: Residual volumetric water content; α, n, m: Adjustment parameters; R^2: Coefficient of correlation
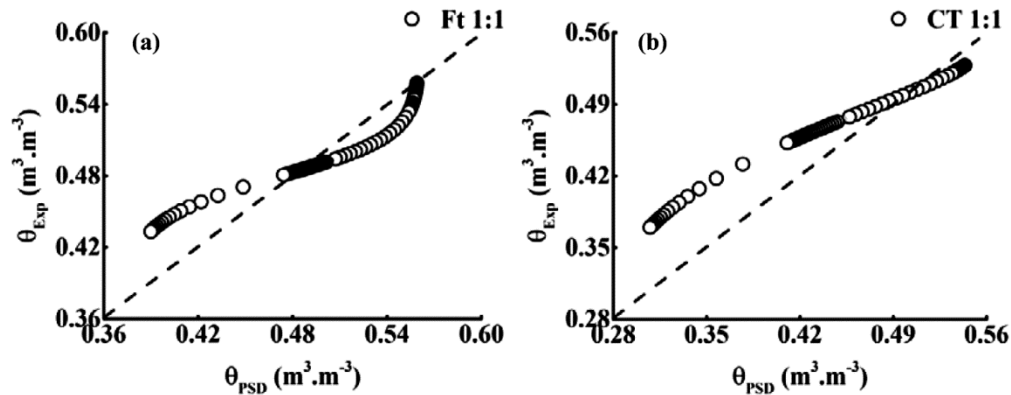
Fig. 3 — (a,b) Relation between the soil water content obtained for Exp and PSD for the different pressure head intervals studied. Ft: Forest; CT: Conventional Tillage.

water content related to pores with smaller sizes (Figs. 3(a-b)[33]. Nonetheless, the proximity of the water contents in relation to the 1:1 line indicates that the method proposed by Yang *et al.*[23] can be successfully used to measure the pF curve based on 3D image analysis. This kind of result is interesting because it allows fast measurements of water retention properties, which are important for the analysis, for instance, of carbon and greenhouse gas sequestration by the soil.

4 Conclusions

The results of this study led to the conclusion that the use of the simulation process based on MIP was quite satisfactory to obtain the partial pF curves of the samples. Samples of soils under different treatements, were analyzed and the procedure, based on simulation using 3D images, was seen to be effective to model the water retention curve. Some deviation was observed for the determinations at high matric potentials (low water contents) as the tomographic technique is limited to the spatial resolution attained at the scan. In our case, it restricted our investigation to the macropore range of investigation, where the pF curves were better correlated. Thus, this methodology is an indication that this approach is suitable to obtain data on retention properties as an alternative to the traditional methods, which are time-consuming and most of the time subject to bias such as hysteresis.

References
1   Dias N M P, Gonçalves D, Leite W C, Brinatti A M, Saab S C & Pires L F, *Powder Technol*, 241 (2013) 36.
2   Pires L F, Roque W L, Rosa J A & Mooney S J, *Soil Till Res*, 191 (2019) 197.
3   Boyle J R & Powers R F, *Earth Syst Environ Sci*, (2013) 1.
4   Pires L F, Auler A C, Roque W L & Mooney S J, *Geoderma*, 362 (2020) 114103.
5   Aziz I, Mahmood T & Islam K R, *Soil Till Res*, 131 (2013) 28.
6   Cássaro F A M, Borkowski A K, Pires L F, Rosa, J A & da Costa Saab S, *Soil Till Res*, 111 (2011) 175.
7   Blanco-Canqui H, Wienhold B J, Jin V L, Schmer M R & Kibet L C, *Soil Till Res*, 170 (2017) 38.
8   Fuentes J P, Flury M & Bezdicek D F, *Soil Sci Soc Am J*, 685 (2004) 1679.
9   Castellini M, Fornaro F, Garofalo P, Giglio L, Rinaldi M, Ventrella, D, Vitti C & Vonella A V, *Water*, 113 (2019) 484.
10 Galdos M V, Pires L F, Cooper H V, Calonego J C, Rosolem C A & Mooney S J, *Geoderma*, 337 (2019) 1126.
11 Borges J A, Pires L F, Cássaro F A, Auler A. C, Rosa J A, Heck R J & Roque W L, *Soil Till Res*, (2019) 25.
12 Lal R & Follett R F, *SSSA Special Publication*, 57 (2009).
13 Silva M L D N, Libardi P L & Gimenes F H S, *Rev Bras Ciên Solo*, (2018) 42.
14 Philippe P, Cuéllar P, Brunier-Coulin F, Luu L H, Benahmed N, Bonelli S & Delenee J Y, *EPJ Web Conf*, EDP Sciences, 140 (2017) 08014.
15 Van G M T, Soil Sci Soc Am J, 44 (1980) 892.
16 Hillel D, *Elsevier Academic Press*, (2004).
17 Pires L F, Bacchi O S & Reichardt K, Soil Till Res, 82 (2005) 89.
18 Yang B H, Wu A X, Miao X X & Liu J Z, *Trans Nonferrous Met Soc China*, 24 (2014) 833.
19 Dong H, Zhang H, Zuo Y, Gao P & Ye G, *Materials*, 11 (2018) 201.
20 Osman A M, Abdel-Monem A M & Abd A El, *Indian J Pure Appl Phys*, 52 (2014) 437.
21 Smet S, Beckers E, Plougonven E, Léonard A & Degré A, *Environ Sci*, 6 (2018) 1.
22 Khan F, Enzmann F, Kersten M, Wiegmann A & Steiner K, *J Soils Sediments*, 12 (2012) 86.
23 Yang Z, Peng X F, Lee D J & Chen M Y, *Environ Sci Technol*, (2008) 1.
24 De Moraes Sá J C, Séguy L, Tivet F, Lal R, Bouzinac S, Borszowskei P R, Briedis C, dos Santos J B, da Cruz Hartman D, Bertoloni C G, Rosa J & Friedrich T, *Land Degrad Dev*, 26 (2015) 531.

25 Soil Survey Staff, USDA-Natural Resources Conservation Service, National Soil Survey Center, (2013).

26 Bauer T, Strauss P, Grims M, Kamptner E, Mansberger R & Spiegel H, *Soil Till Res*, 151 (2015) 28.

27 Jabro J D, Sainju U M, Stevens W B, Lenssen A W & Evans R G, *Arch Agro Soil Sci*, 55 (2009) 633.

28 Reichert J M, Suzuki L E A S, Reinert D J, Horn R & Håkansson I, *Soil Till Res*, 102 (2009) 242.

29 da Costa A B F, Araujo-Junior C F, Caramori P H, Yada I F U & de Conti Medina C, *Afr J Agric Res*, 11 (2016) 3217.

30 Magalhães W D A, Freddi O D S, Lange A, Wruck F J, Silva W M D & Soares M B, *Pesqui Agropecu Bras*, 53 (2018) 351.

31 Swartzendruber D & Hillel D, Edited by Hadas A, Swartzendruber D, Rijtema PE, Fuchs M & Yaron B, Springer, Berlin, Heidelberg, 4 (1973) 3.

32 Pires L F, Brinatti A M, Saab S C & Cássaro F A M, *Appl Radiat Isotopes*, 92 (2014) 37.

33 Pires L F, Cássaro F A M, Saab S C & Brinatti A M, *Nucl Instrum Meth A*, 644 (2011) 68.